RSC Advances

PAPER

Cite this: *RSC Adv.*, 2014, **4**, 46771

Significant enhancement in photocatalytic activity of high quality SiC/graphene core–shell heterojunction with optimal structural parameters†

Wei Lu, Liwei Guo,* Yuping Jia, Yu Guo, Zhilin Li, Jingjing Lin, Jiao Huang and Wenjun Wang

Received 20th June 2014
Accepted 9th September 2014

DOI: 10.1039/c4ra06026a

www.rsc.org/advances

Structure and photocatalytic activity of high quality graphene covered SiC powder (GCSP) composites as metal-free photocatalysts with different sizes and graphene layer numbers are investigated. The results indicate that the GCSP covered with 4–9 layers of graphene reveal outstanding photocatalytic activity enhancement among the other graphene layer numbers. Moreover, it is found that smaller particles have higher activity than the larger ones and more than 730% improvement is achieved by the GCSP derived from 0.5 μm SiC powder relative to the pristine SiC powder, which is more than 6 times of that of photoreduced graphene oxide/SiC composite. Our results demonstrate that it is the high quality graphene and the perfect heterojunction interface between the graphene and SiC particles render the SiC/graphene core–shell heterojunction an outstanding photocatalytic activity, as well as potential for a low cost and metal-free photocatalyst.

1. Introduction

Photocatalysis is a promising way for clean energy and pollution treatment with low cost. In the recent decades, studies on hydrogen production, carbon-dioxide fixation, organics degradation and other applications have been vigorously carried out.[1–4] However, low quantum efficiency due to the strong recombination between the photogenerated electrons and holes is a severe challenge in practical application of the current photocatalytic materials. To suppress the recombination, noble metals like platinum, silver, ruthenium are commonly used as cocatalysts to enhance the separation of photoinduced carriers,[5–7] because the work function of the metals is usually higher than photocatalysts (semiconductors); moreover, the excited electrons will transfer from the photocatalysts to metals when the metals are loaded on catalyst particles. However, the high cost and toxicity of the noble metals are not suitable for a trend of developing metal-free catalysts. It is vital to find inexpensive, earth-abundant materials to replace noble metal catalysts for sustainable development.

Graphene, a full-carbon material, is a potential candidate than the noble metals because of its superior conductivity over the common metals,[8] large specific surface area (SSA, ~2630 $m^2 g^{-1}$),[9] and small light absorption (~2.3%).[10] To date, there are tremendous researches and reports on exploring novel graphene/semiconductor composites for photocatalytic applications, because it has been proved that graphene can obviously enhance the activity of photocatalysts.[11,12] However, the graphene used in those researches was nearly without exception prepared using chemical reduction methods where the most important advantage of graphene with high room temperature mobility ~250 000 $cm^2 V^{-1} s^{-1}$ (ref. 8) has been significantly reduced below 100 $cm^2 V^{-1} s^{-1}$,[13] due to high defect density and considerable function groups. Moreover, the combination of catalyst particles and graphene is realized through physical or chemical mixture with poor and unstable contact interfaces. The limitations in reported graphene-based composites strongly affect the separation of photoinduced carriers. Therefore, exploring high quality graphene combined photocatalyst with ideal graphene–semiconductor heterojunction contact is a promising way to improve photocatalytic performance of graphene–semiconductor composites.

It is known that by thermal decomposition of SiC, graphene can be grown epitaxially on its surface to form a stable heterojunction; moreover, graphene exhibits high carrier mobility (10^3–10^4 $cm^2 V^{-1} s^{-1}$) due to its high quality.[14–17] On the other side, SiC possesses a band gap 2.4 to 3.3 eV depending on its polytype crystalline type, excellent thermal and chemical stabilities,[18] and its compositions are potential photocatalyst materials.[19–23] Therefore, SiC particle combined with epitaxial graphene covered on its surface as an ideal core–shell heterojunction structure that could dramatically enhance the

Research & Development Center for Functional Crystals, Beijing National Laboratory for Condensed Matter Physics, Institute of Physics, Chinese Academy of Sciences, P.O. Box 603, Beijing 100190, China. E-mail: lwguo@iphy.ac.cn; Fax: +86 10 82649646; Tel: +86 10 82649453

† Electronic supplementary information (ESI) available. See DOI: 10.1039/c4ra06026a

photocatalytic activity of SiC, and this composite has great potential to be an active, metal-free and low-cost photocatalyst.

In our previous work, we first reported the fabrication of the graphene covered SiC powder (GCSP) and applied the material for the photodegradation of the dye Rhodamine B (RhB).[24] However, the optimal thickness of the graphene covered on the surface of SiC particle for an outstanding photocatalytic activity has remained a challenge that needs to be solved. The sizes of used SiC particles in that work[24] undoubtedly were too large (~100 μm) to exhibit attractive photocatalytic performance. Therefore, systematic studies on photocatalytic activities of the GCSPs with different sizes of SiC powder and different graphene layer numbers covered on SiC powder are necessary and urgent to explore highly efficient, low cost and metal-free photocatalyst. In addition, a comparative study of the activity of GCSP with that of the reduced graphene oxide (RGO)/SiC composites was also performed to assess the advantage of the GCSP over the RGO/SiC. It was found that a near 730% photoactivity enhancement was achieved to degrade RhB by using the GCSP with optimal structural parameters relative to that of the pristine SiC powder, and there was enhancement more than six times compared with that of the optimal RGO/SiC composite. The experimental results and mechanisms behind were studied and discussed in detail, especially the differences between the GSCP and the RGO/SiC composite. Our results given here confirm that epitaxial high quality graphene is a much better cocatalyst than that of the graphene prepared using the chemical method, and the GCSP composites are promising and have a good potential in photocatalytic applications ascribed to its outstanding photocatalytic activity along with its low cost and environmentally friendly nature.

2. Experimental

2.1. Catalysts synthesis

The SiC particles used in this study were 6H–SiC (band gap ~3.0 eV) powder in four different particle sizes, they are estimated about ~50 μm, ~20 μm, ~5 μm and ~0.5 μm respectively, prepared by mechanical milling and sieving methods. For preparing GCSP, the SiC powder was placed into a graphite crucible with a height less than 1 millimetre to ensure homogeneous GCSP and the crucible was loaded into a home-made high temperature furnace for the fabrication of GCSP material. The synthesis conditions were set at pressure about 10^{-3}–10^{-4} Pa under Ar gas ambient and temperature about ~1400, 1500 and 1600 °C, respectively, for the 0.5, 5 and over 20 μm SiC powder for different time to control graphene thickness. A series of GCSPs, with four sizes covered with different graphene thickness ranging from less than three layers to over 10 layers, were prepared using the abovementioned methods by controlling growth time in about ~5 min, ~10 min and ~15 min. The GCSPs with most graphene thickness less than 3 layers, around 4–9 layers, and over 10 layers were correspondingly represented by GCSP-L, GCSP-M and GCSP-T, respectively.

Comparative photocatalytic experiments using RGO/SiC composite and pure graphene prepared by thorough thermal decomposition of SiC powder were performed. The dry graphene oxide (GO) sheets, which were prepared *via* a modified Hummers method,[22] were dissolved in deionized water by sonicating for 10 hours to prepare 1 mg mL^{-1} GO dispersion. After that, a corresponding amount of 0.5 μm SiC powder was added to the prepared GO dispersion to obtain 0.5, 0.75, 1.0, 1.25, and 1.5 wt% GO/SiC composites with different weight ratios of GO. Moreover, Na_2SO_3 was added to the mixing solution as a hole sacrificial agent in 0.1 mol L^{-1}, and then the solution was aged and stirred vigorous in dark for 6 hours to prepare homogeneous suspension. Then, the suspension was irradiated under 500 W high pressure mercury lamp for 6 hours. By this photocatalytic reducing treatment, the GO was reduced to graphene and SiC particles were deposited onto the RGO sheets. Finally, the RGO/SiC composite was recovered by filtration, rinsed by deionized water and ethanol several times, and dried at 60 °C for 12 hours. The pure graphene in several milligrams was fabricated by high temperature complete thermal decomposition of SiC powder.[25]

2.2. Catalysts characterization

Size and morphology of the GCSP samples were characterized by using field emission scanning electron microscopy (SEM). The characteristics of the graphene formed on the surface of SiC particles were analysed by a high-resolution Raman scattering spectrometer, model HR800 with a 532 nm laser focused to a spot of about 1 μm in diameter. A statistical distribution of graphene layer numbers on each kind of GCSP was analysed based on intensity ratios of G peak of graphene to the attenuation intensity of SiC in their Raman spectrum, which was randomly collected in each set of GCSP to a total of 20 spectra. The graphene grown on the surface of SiC particles were also confirmed by high-resolution transmission electron microscopy (HRTEM) in Tecnai F20 operating at an acceleration voltage of 200 kV. The HRTEM specimen was prepared by grinding the GCSP derived from the 0.5 μm SiC powder into pieces and dispersed with ethanol, then dropped the dispersion on a copper grid after a light baking. The surface compositions of the samples were analysed by using X-ray photoelectron spectroscopy (XPS) in a Quantera SXM Scanning X-ray Microprobe, which consists of a monochromatic Al Kα excitation. The UV-visible diffuse reflectance measurement was performed by using a TU-1901 UV-visible spectrometer. The enhanced photo-induced carrier transfer in the GCSP was tested by electrochemical impedance spectra (EIS) performed in an electrochemical system (CHI-660B, China) by using a three-electrode cell with 0.1 M Na_2SO_4 as electrolyte solution, where ITO electrodes coating the SiC powder in size of 0.5 μm or the GCSP-M derived from 0.5 μm SiC powder on its surface serve as the working electrode, a platinum wire as the counter electrode and a saturated calomel electrode as the reference electrode. Photocurrents from the photocatalysts under a UV lamp on and off were recorded to evaluate the carrier generation and transfer in the photocatalyst.

2.3. Evaluation of photocatalytic activity

The photocatalytic experiments were carried out in an XPA-VII Photochemical Reactor equipped with a 500 W high pressure

mercury lamp and at most 12 quartz tubes around it. To acquire monocolor UV light, 6 filters with center wavelength at 365 nm were applied between the lamp and the tubes in axis-symmetrical sites, which provides a light power density of about 1 mW cm^{-2}. RhB was adopted as the photocatalysis probe due to its high stability under radiation of UV light and sensitivity to visible light absorption due to its intrinsic absorption band at about 553 nm. In each photocatalytic experiment, 50 mL RhB aqueous solution with concentration of 2×10^{-5} mol $liter^{-1}$ (0.02 mM) was filled into each quartz tube together with 50 mg SiC, GCSP, RGO/SiC powder or 3 mg thermal decomposition pure graphene. Before irradiation, the mixture was magnetically stirred in dark for 3.5 hours to approach adsorption–desorption equilibrium. The mixtures were then irradiated by 365 nm UV light at room temperature and ambient pressure, while stirring to keep catalyst particles homogenously dispersed in the solution. Moreover, a blank comparative experiment was also conducted where no catalyst was in the solution. The blank experiments at the same conditions showed no degradation in the absence of catalyst or light irradiation as can be seen in Fig. S1 in the ESI.†

During UV light irradiation, about 5 mL of the suspension was taken out from the tube at a given time intervals of about 30 min in sequence for subsequent analysis of target dye concentration after centrifuging. Absorption spectra of the suspensions were collected by a TU-1901 UV-visible spectrometer. The photocatalytic activity of the GCSP was evaluated from the intrinsic absorption band (at 553 nm) intensity ratio of the remnant RhB after UV light illumination to that of the RhB in parent solution.

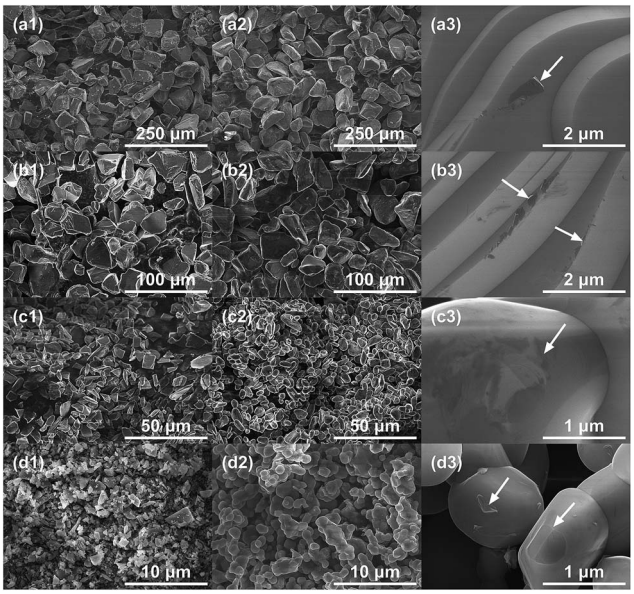

Fig. 1 SEM images of the pristine SiC powder in sizes of 50, 20, 5 and 0.5 μm (a1–d1), respectively, and the corresponding as grown GCSP-Ms with 4–9 layers graphene (a2–d2) and their magnified images (a3–d3), respectively. The arrows in the magnified images mark the peeled graphene or the graphene wrinkle.

3. Results and discussion

3.1. Characterization of catalysts

Fig. 1 shows the SEM images of the as grown GCSP-Ms in sizes of 50, 20, 5 and 0.5 μm as typical examples of GCSP together with their pristine SiC powder. The morphology of the comparative RGO/SiC composite is shown in the Fig. S2 in ESI.† Fig. 1(a1)–(d1), (a2)–(d2) and (a3)–(d3) are to the pristine SiC powder, the GCSP-Ms and their magnified images, respectively. Observing Fig. 1(a1)–(d1), it can be seen that pristine SiC particles show sharp edges. However, the morphologies of the GCSP-Ms shown in Fig. 1(a2)–(d2) exhibit a trend of its edges rounded with the size decreasing. In the case of the smallest size of 0.5 μm, particles nearly became balls with size about 1 μm through merging of the small particles to decrease the surface energy. Some small particles accumulated into even large cluster as shown in Fig. 1(d2) and (d3). The obvious merging phenomena of the SiC particles after high temperature treatment happened only in the powder with particle size less than about 1 μm, but not in others with larger sizes. The phenomena can be well explained from the point of view of thermodynamics.[26,27] The small particles will coalesce into large ones to decrease surface energy at high temperature accompanied by a process of grain size distribution becoming more uniform. The smaller the particle size, the faster the process. However, the coalescence of the small particles reduced not only the surface energy but also the SSA as well as surface dangling bonds, which is adverse to photocatalytic activity. Thus, avoiding coalescence of the small particles is our task in the next study. Although the morphology images shown here are about GCSP-M, similar phenomena, including the rounding of the particle edges and coalescing of the small particles, were also observed in the other prepared GCSPs. Fig. 1(a3)–(d3) shows the magnified images of SiC particles after graphene formed on the particle surface. Steps and terraces can be seen clearly on the surfaces of the GCSPs in a size more than 5 μm, but not in the smaller ones. The covered graphene layer was smooth and wraps SiC particle tightly with perfect contact interfaces, which were clearly observed in all GCSPs with some graphene peeled off from the SiC surface or wrinkles appeared on the surface as seen in the area marked with the arrows in Fig. 1(a3)–(d3).

The graphene covered on the surface of SiC particles was confirmed by Raman scattering measurement. Fig. 2(a) shows the Raman scattering spectra of the pristine SiC powder and the GCSP-i (i = L, M and T, respectively). Raman fingerprint peaks of graphene called as G and 2D peaks were well identified and located at 1582 ± 3 and 2701 ± 6 cm^{-1} depending on layer numbers of graphene, strain and doping in graphene induced by SiC,[28,29] which strongly indicates the graphene were coupling with SiC. In addition to the strong G and 2D peaks from graphene, a weak D peak also appeared. The inset in Fig. 2(a) is the Raman signal of graphene on GCSP-M after subtracting SiC signal. The intensity ratio of I_D/I_G was about 0.13, smaller than that of the graphene prepared by chemical method whose ratio is about 1 or even much higher,[22,30] such as that in GO and RGO (Fig. S3 in ESI†). This indicates that the quality of graphene on

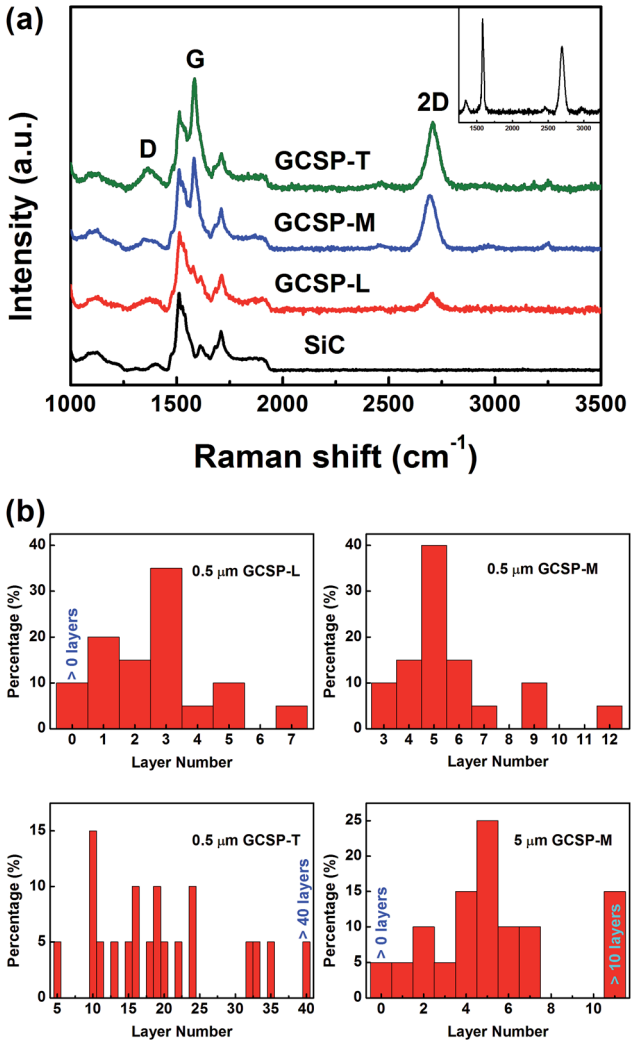

Fig. 2 (a) Typical Raman spectra of GCSP-i (i = L, M and T) together with that of the pristine SiC powder. The inset is the Raman spectrum of GCSP-M after subtracting SiC signal. (b) A roughly statistical distribution of graphene layer numbers in each of GCSP-i derived from 0.5 μm SiC powder and the GCSP-M derived from 5 μm SiC powder, respectively.

GCSP is much higher compared with the graphene prepared by chemical method.

In addition, graphene layer numbers on the GCSP was also analysed based on Raman scattering data, which proved to be an reliable method to determine the layer numbers of epitaxial graphene on SiC.[29,31–33] Fig. 2(b) gives the statistic distributions of the graphene layer numbers from random collected 20 Raman spectrum data from each of GCSP-i (i = L, M and T, respectively) derived from 0.5 μm SiC powder or from the GCSP-M derived from 5 μm SiC powder, where the graphene layer numbers were estimated according to the intensity ratio of the I_G to I_{SiC} located at about 1515 cm^{-1}. The intensity of Raman peaks has been widely used to roughly estimate layer numbers of graphene on SiC intuitively.[29,31] Our estimation on graphene thickness was in good agreement with other reports.[32,33] According to the statistic results shown in Fig. 2(b), it can be

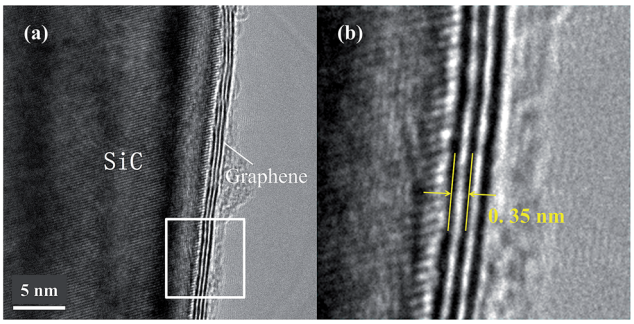

Fig. 3 (a) HRTEM image of a GCSP-M derived from 0.5 μm SiC particles. (b) A magnified image of the selected square in (a).

seen that the major graphene layer numbers were around 3 layers in GCSP-L, 5 layers in the GCSP-M, and over 10 layers in the GCSP-T. It was also seen from Fig. 2(b) that for the GCSP-M in different SiC particle sizes of about 0.5 and 5 μm, the distributions of graphene thickness were similar, which is ascribed to the similar growth dynamics for graphene.

The graphene grown on the surface of SiC particle was confirmed by HRTEM analysis on GCSP with few layer graphene as shown in Fig. 3, where three graphene monolayers are clearly seen. It should be noted the graphene layers were attached on the SiC surface tightly without interruption in the visible region, indicating a continuous high quality graphene. The interlayer space of the graphene layers was about 0.35 nm as scaled in Fig. 3(b), well matching with other reports for the graphene with weak interaction.[16,17,34–36] In addition, it should be stressed that the fabrication procedure used here for the GCSP can ensure each particle in the GCSP with similar physical features as if the loaded quantity of SiC powder in a crucible was less than 1 mm in height. The similar properties in each set of particles were supported by the Raman scattering results shown in Fig. 2.

3.2. Photocatalytic performance on degradation of RhB

The photocatalytic activities of SiC and GCSPs were tested by photodegradation of RhB, where the characteristic absorption band of RhB at 553 nm was chosen as the monitoring parameter to evaluate the remnant concentration of RhB. The detailed absorption spectra are shown in Fig. S4 (ESI†). Here, the evolution of the relative remnant concentration of the RhB aqueous solution under the 365 nm UV irradiation in the case of containing the GCSPs or the pristine SiC powders in four sizes are shown in Fig. 4. It can be seen that the degradation rates of GCSPs to RhB were very fast compared with the pristine SiC powder, and even close or catch up to other nano-catalysts including TiO_2.[37–41] Theoretically, the GCSPs have great potential to surpass the current high efficiency photocatalysts if their SSA are further enlarged with reducing particle sizes and optimal graphene layer numbers. Fig. 4(a)–(d) show that the GCSP-M possess the most outstanding degradation activities no matter the sizes of the GCSPs. The results, indicates that graphene layer number is a dominant factor in determining the photocatalytic performance of the composites. In GCSP-L, there were some regions on surface of SiC particle, which are not

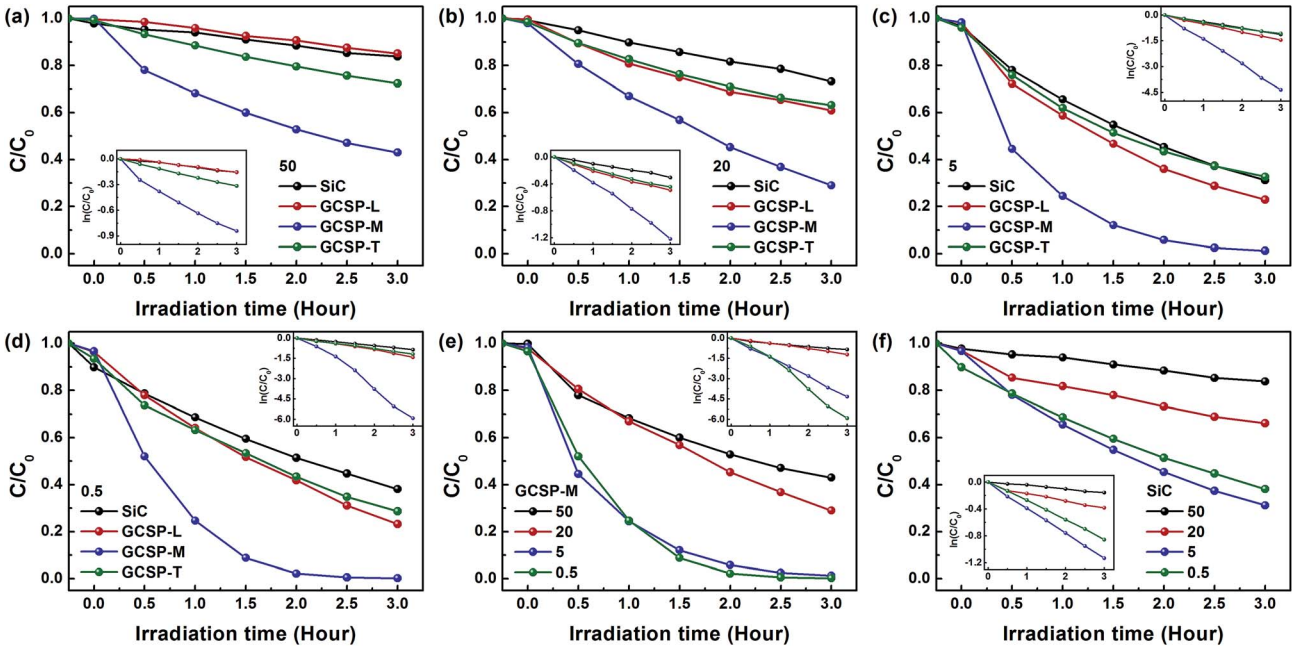

Fig. 4 Time profiles of RhB photodegradation with the GCSPs covered with different graphene thicknesses together with pristine SiC powder, in sizes of (a) 50 μm, (b) 20 μm, (c) 5 μm and (d) 0.5 μm, respectively; (e) and (f) are that of the GCSPs with the optimal graphene thickness and the pristine SiC powders in the four sizes, respectively, C_0 is defined as the concentration of parent solution. The insets are the natural logarithm curves corresponding to the concentration ratio, where the unit of abscissa is hour.

covered graphene due to the disparity of graphene growth rates on different SiC crystal planes,[17] making the effective area covered with graphene reduced and rendering a poor carrier separation. This leads to a relative low reactive activity compared with the GCSP-M. While in the case of excessively thick graphene as the GCSP-T, the SiC particles were completely covered with the thick graphene and the effective UV light absorption by SiC particles was cut down. As is well known, the absorbance of graphene monolayer is about 2.3%.[10] The thicker graphene on the surface of SiC absorbs more light, which leads to a decrease in the incident light that penetrates into the SiC particles. To support the analysis, absorbance spectra were collected on the GCSP samples together with the pristine and annealed SiC powder, as shown in the Fig. S5 (ESI†). It was observed that the thicker the graphene covered on the SiC, the stronger the absorbance of the sample in the whole wavelength range. In addition, the conductivity of carriers was relatively poor between graphene interlayers. Hence, the thicker the graphene, the less the photogenerated carriers in the SiC transfer to the out graphene layer, that directly determines the number of carriers to take part in redox reaction. Therefore, an optimal graphene thickness is needed to explore in detail. At present, the GCSP-M with about 4–9 layers graphene reveals an outstanding photocatalytic activity. This catalyst also exhibits relatively good stability to maintain its photoactivity after five complete cycles, as shown in Fig. S6 (ESI†).

In Fig. 4(e) and (f), a phenomenon is found that the degradation efficiency of the catalyst enhances with decreasing particle size no matter the catalytic particles are the GCSP or the pristine SiC powder, except the case of 0.5 μm pristine SiC powder. The dominant mechanism behind the phenomenon was the increased SSA, which was equivalent to the increase of photocatalytic reaction active sites and effective light absorption area. Since the SSA is inversely proportional to its size, the smaller the particle size, the larger the SSA, and the more reactive sites and effective absorption area. On the other hand, the abnormal photocatalytic activity deterioration in 0.5 μm pristine SiC powder may be ascribed to the surface defects or adsorbed impurities on its surface. In as-purchased commercial product of pristine SiC powder, there are more or less surface defects and surface contaminations, which was supported by the XPS spectrum shown in Fig. S7 (ESI†). The defects will trap the photogenerated carriers, resulting in a decrease of free carriers and a deterioration of photocatalytic activity. Comparatively, the photocatalytic activities of GCSPs derived from 0.5 μm were comparable with or even higher than those of 5 μm GCSPs, because the surface defects on 0.5 μm particles have been reduced during high temperature growth of graphene and SSA was higher in the GCSP derived from the 0.5 μm SiC powder than that from the 5 μm SiC powder, even though the 0.5 μm SiC particles merge into large ones with size of 1–3 μm. Therefore, the GCSPs derived from 0.5 μm SiC powder display a little better photocatalytic activity over that of 5 μm particles.

In addition, a comparative study was performed on photocatalytic activity between the annealed SiC powder without graphene formed on its surface and the pristine SiC powder in sizes of 5 μm and 0.5 μm, respectively. The morphologies of the annealed SiC powder are similar to the same sized GCSP as shown in Fig. 1(c2) and (d2). However, the photodegradation rate shown in Fig. S8 (ESI†) suggests that the annealed SiC

powder exhibited an even bad photocatalytic activity compared with the pristine ones no matter their sizes. It was considered that there were more active sites and the impurities like free C and Fe atoms (Fig. S7 in ESI†) acting as cocatalyst that existed on the surface of the pristine SiC powder, both of which contribute photocatalytic activity compared with that of the annealed SiC powder. Moreover, high temperature annealing made the SSA of SiC particles reduced, also resulting in lower reaction rate. This indirectly supports the fact that it was the graphene covered on the surface of SiC particles that provides the GCSP a tremendous enhancement in photocatalytic activity.

The insets in Fig. 4 are the time profiles of $\ln(C/C_0)$, the slopes indicate the rates of first-order reactive kinetic, which intuitively quantifies the photocatalytic activity of catalyst. The rate constants of the GCSP-i (i = L, M and T, respectively), the annealed and the pristine SiC powder for degradation of RhB are shown in Fig. 5. It is noted the GCSP-M exhibits an outstanding photocatalytic activity enhancement compared with others, although all other GCSPs also exhibited enhanced photocatalytic activity more or less. GCSP-M derived from the 0.5 μm SiC powder achieved near 730% improvement in efficiency compared with the pristine SiC powder (even ~1540% compared with the annealed SiC powder, which was the real matrix of the GCSP), and the enhancement of photoactivity for the other GCSP-Ms were also over 380% compared with the pristine SiC powder. The difference of activity enhancements in similar graphene thickness but different sized GCSP-M was probably due to the difference in SSA and in uniformity of graphene thickness as seen in Fig. 2(b). Our results indicate that the 4–9 layers graphene exhibits outstanding photoactivity by combining the advantages of graphene and SiC particles.

To understand the advantages of the GCSP as advanced photocatalytic material, contrast tests on the photocatalytic activities of the pure graphene prepared by thermal decomposition of SiC and the RGO/SiC compositions in different weight ratios of graphene to the SiC powder are performed under the same conditions as for the GCSP. The photocatalytic rate is shown in Fig. S9 (ESI†) and the remnant concentration profiles are shown in Fig. 6. In Fig. 6(a), the 3 mg pure graphene catalyst shows no discernible photocatalytic activity, in addition to a

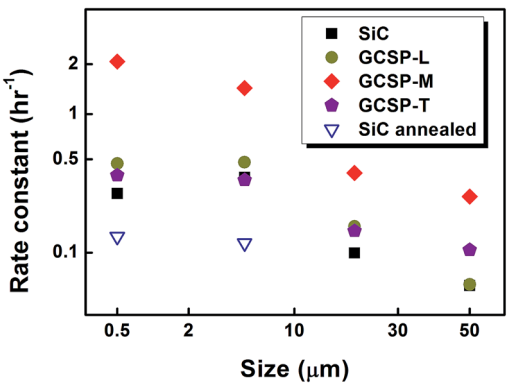

Fig. 5 The rate constants of the first-order reaction kinetics in degradation of RhB by SiC powders and GCSPs.

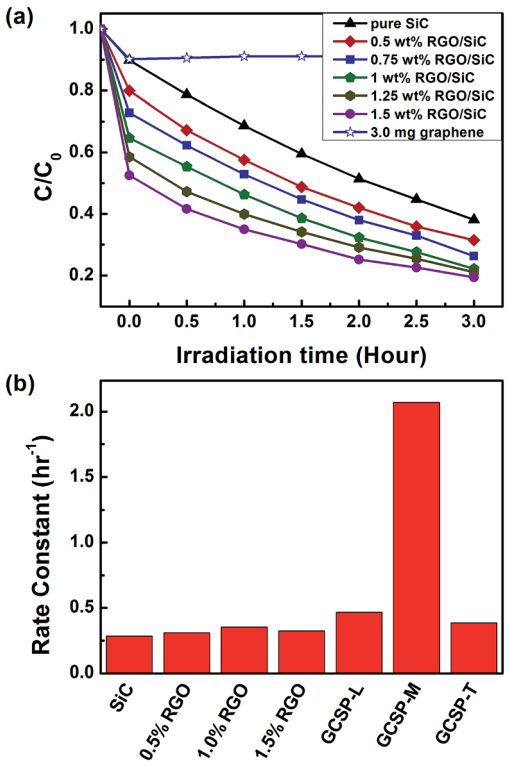

Fig. 6 (a) Time profiles of RhB photodegradation with the RGO/SiC composites in RGO weight ratio from 0% to 1.5% together with 3.0 mg pure thermal decomposition graphene sheets. (b) The degradation rate constants for 0.5 μm pristine SiC, corresponding RGO/SiC composites and GCSP-i (i = L, M and T), respectively.

near 10% adsorption to RhB molecular. This strongly indicates the enhancement of photocatalytic activity in our GCSP relies on the graphene–SiC heterojunction but not on graphene itself. In addition, it was seen that the adsorption of RGO/SiC composite to RhB molecular was increasing considerably from 20% to near 50% with increase in RGO weight ratio from 0.5% to 1.5% as confirmed by an obvious variation of dye concentration before irradiation. However, the degradation rates of the composites were similar with a maximum in graphene weight ratio 1.0% as evidenced by Fig. S9 (ESI†), which was only about 120% larger compared with that of the pristine SiC powder as deduced from the data in Fig. 6(b). The results are in good agreement with other reports.[22]

Compared with the RGO/SiC composites, the GCSPs derived from 0.5 μm SiC powder have significant enhancement in activities, especially for the GCSP-M, as shown in Fig. 6(b). The degradation rate of the GCSP-M was over 6 times as that of optimal RGO/SiC in 1.0 wt% RGO. The experimental results sufficiently proved that high quality heterojunction material of semiconductor–graphene core–shell structure is far superior to conventional graphene-based composite photocatalyst.

3.3. Mechanism of photoactivity enhancement of the GCSP

The higher photoactivity of GCSP over RGO/SiC can be understood from the three fundamental aspects in influencing

photocatalytic activity: extending the light absorption range, enhancing adsorptivity, and efficient charge separation and transfer.[42,43] Some researchers reported that graphene extends the absorption range of semiconductor due to surface hybrid.[42,43] Because the irradiation used in this experiment was monochromatic 365 nm; therefore, extending absorption was not considered as a factor in our experiment.

High adsorptivity of catalyst can facilitate the direct redox reactions of organics. However, as seen in Fig. 4 and 6(a), the adsorption of the high active GCSP to RhB was far lower than that of RGO/SiC, which should result from the difference in graphene qualities. The RGO contains high density of defects and functional groups,[12,13] which provide extra combining sites for the extrinsic molecules besides π–π conjugation between aromatic structures of molecule and graphene, and which at the same time deteriorate carrier conductivity considerably. The significant deterioration of carrier conductance counteracted the benefit of enhanced adsorptivity.

Except the former two cases, the efficient charge separation and transfer are the major contributions in our experiments. As seen in HRTEM image of Fig. 3, graphene is epitaxially grown on surface of SiC particle, in other words, each catalyst particle in GCSP is composed of SiC core and graphene shell, like a ball-shaped heterojunction. In the heterojunction interface, the conduction band of SiC was about 1.5 eV higher than the Fermi level of graphene,[12,19,20,23] which acts as a large internal electrical field to drive the photogenerated carriers in the SiC particles migrating to graphene rapidly to attend redox action. Moreover, the migration of carrier in graphene is fast because of the excellent transport properties of graphene grown on SiC,[16] which promote carriers finding active sites to react with organic molecules. It is the natural combination of the advanced graphene, the perfect heterojunction interface and the building of strong internal electrical field in heterojunction interface that makes each particle a highly efficient photocatalyst as well as provides the GCSP with an outstanding photocatalytic activity.

The enhanced carrier transfer in the GCSP was proved through the study of EIS and photocurrent intensity spectroscopy of the GCSP-M derived from the 0.5 μm SiC powder and the pristine SiC powder. Fig. 7(a) shows the EIS Nyquist plot, the impedance arc radius of the GCSP-M was much smaller than that of pristine SiC powder, which indicates the surface and interface resistances of the GCSP-M were reduced obviously compared with those of the pristine SiC powder. The reduced resistance in the GCSP was ascribed to the high conductivity of the covered graphene and the tight coupling between graphene shell and SiC core. In addition, photocurrents were measured for the GCSP-M and SiC powder electrodes to investigate the carrier transfer as shown in Fig. 7(b). A rapid and strong photocurrent response was clearly observed in the GCSP-M electrode, which was about three times as high as that of the pristine SiC powder electrode. The photocurrent enhancement in the GCSP-M photocatalyst indicates an enhanced separation between the photogenerated electrons and holes, which could be attributed to the large internal electrical field building at the interface of the SiC and graphene as discussed in our earlier work[24] and the high mobility of carrier in the graphene.[16]

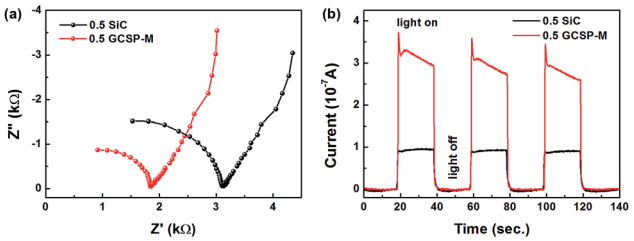

Fig. 7 (a) Nyquist plots of EIS and (b) photocurrents for the pristine SiC powder in size 0.5 μm (black curve) and it derived GCSP-M (red curve) electrodes under UV illumination, respectively.

Based on the analysis above, the photocatalytic process of GCSP degradation RhB can be further explained as follows. The core–shell heterojunction and high quality graphene rapidly separate and transport excited electrons in SiC to the outside. Then, in the redox reaction processes, due to the relatively negative conduction band potential of 6H–SiC to other semiconductors,[12,19,20,23] the hole induced reactions were weaker here. Therefore, electron induced reactions were the major process in our photocatalytic experiment. In the process, the dissolved oxygen in the solution as electron acceptor was vital for organic photodegradation. The oxygen captures the photoinduced electron to form the active oxygen species (*e.g.* superoxide anion radical or singlet oxygen), which are vigorous oxidizing reagents to organics.[42,44–46] If without oxygen, then the accumulated space charge layer in graphene–SiC heterojunction will inhibit the carrier transfer further, leading to significant lowering of redox reaction rate. Therefore, the separated electrons were continually captured by dissolved oxygen in RhB solution to form active oxygen species to decompose RhB, and the residual holes directly oxidize the dye molecules through the defect sites of graphene. The schematic of the process is illustrated in Scheme 1.

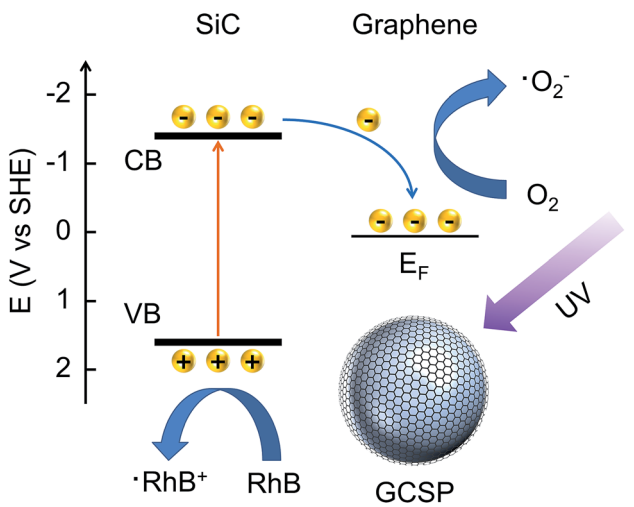

Scheme 1 Suggested mechanism for the photocatalytic degradation of RhB by GCSP under UV irradiation. The photoinduced electrons in SiC particle are transferred to the graphene shell rapidly, then captured by oxygen in solution to produce active oxygen species. The RhB can be decomposed either by the free holes in the SiC through the defect sites of graphene or by the active oxygen species.

4. Conclusions

The GCSPs with different graphene thicknesses and SiC particle sizes were prepared *in situ* by annealing 6H–SiC powder at high temperature under high vacuum environment. High quality graphene were tightly attached on the surface of each SiC particle to form a core–shell heterojunction smart structure. The photocatalytic activity measurements on the GCSPs in degradation of RhB by UV irradiation as well as EIS and photocurrent analysis indicate that the high quality SiC/graphene core–shell heterojunction significantly promotes the separation of photoinduced electrons and holes, and results in more carriers participating in redox reactions. It was found that the optimal graphene thickness was about 4–9 layers for high photocatalytic performance in the present experiment. Moreover, the smaller the size of the GCSP, the better the performance of the GCSP is in photocatalysis. A ~730% enhancement in photocatalytic activity was achieved, which was about 6 times better than that of the RGO/SiC composites. In our experiments, the minimum size of the GCSP was about 1–3 μm, derived from SiC powder in average size about 0.5 μm. The coalescence and cluster of small sized SiC particles at high temperature prevented us from obtaining GCSPs with even smaller size at present. With further optimization procedure for GCSP, such as suppressing the coalescence of the small sized particles and control uniformity in graphene layer number, the photocatalytic activity of the GCSPs will be even improved to meet the requirement for metal-free, high efficiency catalyst.

Acknowledgements

Wei Lu, one of authors, is grateful to Prof. Yongfa Zhu and PhD candidate, Yanhui Lu, in Department of Chemistry, Tsinghua University, for the great support in electrochemical measurements, and Prof. Wenxia Yuan and PhD candidate, Xiaopeng Zeng, in Department of Chemistry, University of Science and Technology, Beijing, for providing GO material. The work is partly supported by the grants from the National key Basic Research Program of China (nos 2011CB932700 and 2013CBA01603), and the National Natural Science Foundation of China (nos 51072223 and 51272279).

Notes and references

1 X. Chen, S. Shen, L. Guo and S. S. Mao, *Chem. Rev.*, 2010, **110**, 6503–6570.
2 S. C. Roy, O. K. Varghese, M. Paulose and C. A. Grimes, *ACS Nano*, 2010, **4**, 1259–1278.
3 K. Rajeshwar, M. E. Osugi, W. Chanmanee, C. R. Chenthamarakshan, M. V. B. Zanoni, P. Kajitvichyanukul and R. Krishnan-Ayer, *J. Photochem. Photobiol., C*, 2008, **9**, 171–192.
4 A. Fujishima, T. N. Rao and D. A. Tryk, *J. Photochem. Photobiol., C*, 2000, **1**, 1–21.
5 R. Konta, T. Ishii, H. Kato and A. Kudo, *J. Phys. Chem. B*, 2004, **108**, 8992–8995.
6 L. Jing, D. Wang, B. Wang, S. Li, B. Xin, H. Fu and J. Sun, *J. Mol. Catal. A: Chem.*, 2006, **244**, 193–200.
7 X. Zong, H. Yan, G. Wu, G. Ma, F. Wen, Y. Wang and C. Li, *J. Am. Chem. Soc.*, 2008, **130**, 7176–7177.
8 A. K. Geim, *Science*, 2009, **324**, 1530–1534.
9 M. D. Stoller, S. Park, Y. Zhu, J. An and R. S. Ruoff, *Nano Lett.*, 2008, **8**, 3498–3502.
10 F. Bonaccorso, Z. Sun, T. Hasan and A. C. Ferrari, *Nat. Photonics*, 2010, **4**, 611–622.
11 N. Zhang, Y. Zhang and Y.-J. Xu, *Nanoscale*, 2012, **4**, 5792–5813.
12 Q. Xiang, J. Yu and M. Jaroniec, *Chem. Soc. Rev.*, 2012, **41**, 782–796.
13 K. S. Novoselov, V. I. Fal'ko, L. Colombo, P. R. Gellert, M. G. Schwab and K. Kim, *Nature*, 2012, **490**, 192–200.
14 K. V. Emtsev, F. Speck, Th. Seyller, L. Ley and J. D. Riley, *Phys. Rev. B: Condens. Matter Mater. Phys.*, 2008, **77**, 155303.
15 C. Riedl, C. Coletti and U. Starke, *J. Phys. D: Appl. Phys.*, 2010, **43**, 374009.
16 J. Hass, F. Varchon, J. E. Millán-Otoya, M. Sprinkle, N. Sharma, W. A. de Heer, C. Berger, P. N. First, L. Magaud and E. H. Conrad, *Phys. Rev. Lett.*, 2008, **100**, 125504.
17 M. Sprinkle, J. Hicks, A. Tejeda, A. Taleb-Ibrahimi, P. Le Fèvre, F. Bertran, H. Tinkey, M. C. Clark, P. Soukiassian, D. Martinotti, J. Hass and E. H. Conrad, *J. Phys. D: Appl. Phys.*, 2010, **43**, 374006.
18 C. Persson and U. Lindefelt, *Phys. Rev. B: Condens. Matter Mater. Phys.*, 1996, **54**, 10257.
19 T. Inoue, A. Fujishima, S. Konishi and K. Honda, *Nature*, 1979, **277**, 637–638.
20 B. R. Eggins, P. K. J. Robertson, E. P. Murphy, E. Woods and J. T. S. Irvine, *J. Photochem. Photobiol., A*, 1998, **118**, 31–40.
21 V. Keller and F. Garin, *Catal. Commun.*, 2003, **4**, 377–383.
22 J. Yang, X. Zeng, L. Chen and W. Yuan, *Appl. Phys. Lett.*, 2013, **102**, 083101.
23 C. E. Nebel, *Nat. Mater.*, 2013, **12**, 780–781.
24 K. Zhu, L. Guo, J. Lin, W. Hao, J. Shang, Y. Jia, L. Chen, S. Jin, W. Wang and X. Chen, *Appl. Phys. Lett.*, 2012, **100**, 023113.
25 L. Chen, L. Guo, Y. Wu, Y. Jia, Z. Li and X. Chen, *RSC Adv.*, 2013, **3**, 13926–13933.
26 O. Gülseren, F. Ercolessi and E. Tosatti, *Phys. Rev. B: Condens. Matter Mater. Phys.*, 1995, **51**, 7377–7380.
27 J.-H. Shim, B.-J. Lee and Y. W. Cho, *Surf. Sci.*, 2002, **512**, 262–268.
28 J. Röhrl, M. Hundhausen, K. V. Emtsev, T. Seyller, R. Graupner and L. Ley, *Appl. Phys. Lett.*, 2008, **92**, 201918.
29 L. M. Malard, M. A. Pimenta, G. Dresselhaus and M. S. Dresselhaus, *Phys. Rep.*, 2009, **473**, 51–87.
30 Y. Zhang, N. Zhang, Z.-R. Tang and Y.-J. Xu, *Phys. Chem. Chem. Phys.*, 2012, **14**, 9167–9175.
31 S. Shivaraman, M. V. S. Chandrashekhar, J. J. Boeckl and M. G. Spencer, *J. Electron. Mater.*, 2009, **38**, 725–730.
32 C. Faugeras, A. Nerrière, M. Potemski, A. Mahmood, E. Dujardin, C. Berger and W. A. de Heer, *Appl. Phys. Lett.*, 2008, **92**, 011914.
33 D. S. Lee, C. Riedl, B. Krauss, K. von Klitzing, U. Starke and J. H. Smet, *Nano Lett.*, 2008, **8**, 4320–4325.

34 J. Borysiuk, J. Sołtys, R. Bożek, J. Piechota, S. Krukowski, W. Strupiński, J. M. Baranowski and R. Stępniewski, *Phys. Rev. B: Condens. Matter Mater. Phys.*, 2012, **85**, 045426.
35 J. Borysiuk, R. Bożek, K. Grodecki, A. Wysmołek, W. Strupiński, R. Stępniewski and J. M. Baranowski, *J. Appl. Phys.*, 2010, **108**, 013518.
36 J. Borysiuk, J. Sołtys and J. Piechota, *J. Appl. Phys.*, 2011, **109**, 093523.
37 P. Qu, J. Zhao, T. Shen and H. Hidaka, *J. Mol. Catal. A: Chem.*, 1998, **129**, 257–268.
38 H. Fu, S. Zhang, T. Xu, Y. Zhu and J. Chen, *Environ. Sci. Technol.*, 2008, **42**, 2085–2091.
39 Y. Xia and L. Yin, *Phys. Chem. Chem. Phys.*, 2013, **15**, 18627.
40 C. C. Pei and W. W. F. Leung, *Sep. Purif. Technol.*, 2013, **114**, 108–116.
41 M. F. Abdel-Messih, M. A. Ahmed and A. S. El-Sayed, *J. Photochem. Photobiol., A*, 2013, **260**, 1–8.
42 L.-W. Zhang, H.-B. Fu and Y.-F. Zhu, *Adv. Funct. Mater.*, 2008, **18**, 2180–2189.
43 H. Zhang, X. Lv, Y. Li, Y. Wang and J. Li, *ACS Nano*, 2010, **4**, 380–386.
44 Z. Xiong, L. L. Zhang and X. S. Zhao, *Chem.–Eur. J.*, 2011, **17**, 2428–2434.
45 A. C. S. Samia, X. Chen and C. J. Burda, *J. Am. Chem. Soc.*, 2003, **125**, 15736–15737.
46 J. S. Lee, K. H. You and C. B. Park, *Adv. Mater.*, 2012, **24**, 1084–1088.